PHYSICAL REVIEW D **82,** 054003 (2010)

Hadron multiplicity in pp and AA collisions at LHC from the color glass condensate

Eugene Levin[1,2] and Amir H. Rezaeian[1]

[1]*Departamento de Física, Universidad Técnica Federico Santa María, Avda. España 1680, Casilla 110-V, Valparaiso, Chile*

[2]*Department of Particle Physics, Tel Aviv University, Tel Aviv 69978, Israel*

(Received 19 July 2010; published 1 September 2010)

We provide quantitative predictions for the rapidity, centrality and energy dependencies of inclusive charged-hadron productions for the forthcoming LHC measurements in nucleus-nucleus collisions based on the idea of gluon saturation in the color-glass condensate framework. Our formulation gives very good descriptions of the first data from the LHC for the inclusive charged-hadron production in proton-proton collisions, the deep inelastic scattering at the Hadron-Elektron-Ring-Anlage at small Bjorken x, and the hadron multiplicities in nucleus-nucleus collisions at the Relativistic Heavy Ion Collider.

DOI: 10.1103/PhysRevD.82.054003 PACS numbers: 25.75.Ag, 13.60.Hb, 25.75.−q, 25.75.Nq

I. INTRODUCTION

It has been widely discussed that QCD predicts at high-energy formation of a new state of matter, the so-called color-glass condensate (CGC) [1]. In this state, the density of quarks and gluons ρ with transverse momenta less that Q_s reaches a high value, namely $\rho \propto 1/\alpha_s(Q_s) \gg 1$ where α_s is the strong coupling constant and Q_s is a new momentum scale (saturation momentum) that increases with energy. Therefore, $\alpha_s(Q_s) \ll 1$ and this fact allows us to treat this system on solid theoretical basis. One of the most characteristic and qualitative consequences of the CGC is the emergence of a new mechanism for hadron production at high energy. In this approach, the process of secondary hadron production goes in two stages: production of gluon minijet with a typical transverse momentum Q_s; and the decay of gluon minijets into hadrons.

The CGC picture for the hadron production has passed two critical tests. First, it explains the main features of hadron multiplicity in heavy ion-ion collisions at the Relativistic Heavy Ion Collider (RHIC) [Kharzeev-Levin-Nardi (KLN) papers [2]); and it predicts the inclusive hadron production in proton-proton (pp) collisions [3] at the LHC which was recently confirmed experimentally by the CMS Collaboration at $\sqrt{s} = 7$ TeV [4] and the lower LHC energies [5–7], see also Ref. [8]. The ion-ion collisions at the LHC will lead to a crucial test of the CGC approach. Indeed, the KLN success [2] in the description of RHIC data shows that we are dealing with scatterings of dense partonic systems even at rather low energies. At higher energies we expect that the density of scattering systems increases resulting in more transparent and unambiguous evidence for the creation of the CGC.

In this paper we wish to extend our approach [3] to ion-ion (AA) collisions at the LHC. As it was discussed in Ref. [3], we improve the KLN approach [2] in various ways incorporating the unintegrated gluon density that describes the Hadron-Elektron-Ring-Anlage (HERA) data at small Bjorken x. We also include our knowledge on proton-proton scatterings at the LHC to make our prediction more reliable. In particular, we re-calculate the saturation momentum for nuclei from the saturation momentum in the proton target obtained from deep-inelastic scattering (DIS) data at HERA and confront it with the RHIC's gold-gold data. On the contrary, in the KLN approach [9], the LHC saturation momentum was found via an extrapolation of the energy dependence of the saturation scale at RHIC in the Balitsky-Fadin-Kuraev-Lipatov region.

In the next section, we discuss the k_T factorization and our main formulation for the inclusive hadron production in pp and AA collisions. In particular, we introduce the impact-parameter dependent saturation scale for a proton and a nuclear target. Section III is devoted to comparison with the experimental data and to discussion of various predictions for the LHC energies. Finally, we conclude in Sec. IV.

II. MAIN FORMULATION

The gluon-jet production in nucleus-nucleus collisions can be described by the k_T factorization given by [10],

$$\frac{d\sigma}{dyd^2p_T} = \frac{2\alpha_s}{C_F}\frac{1}{p_T^2}\int d^2\vec{k}_T \phi_A^G(x_1;\vec{k}_T)\phi_A^G(x_2;\vec{p}_T - \vec{k}_T), \tag{1}$$

where $x_{1,2} = (p_T/\sqrt{s})e^{\pm y}$, p_T, and y are the transverse momentum and rapidity of the produced gluon minijet. $\phi_A^G(x_i;\vec{k}_T)$ denotes the unintegrated gluon density and is the probability to find a gluon that carries x_i fraction of energy with k_T transverse momentum in the projectile (or target) nucleus A. We defined $C_F = (N_c^2 - 1)/2N_c$ where N_c denotes the number of colors.

The k_T factorization has been proven [10] for the scattering of a diluted system of parton with a dense one. Such a process can be characterized by two hard scales: the transverse momentum of produced particle p_T and a saturation scale which are both larger than the soft interaction scale μ. The ion-ion scattering is a typical example in which we have three scales: p_T and two saturation scales for the projectile and the target. The k_T factorization might be then

violated only at low x_1 and x_2, and when p_t is smaller than both saturation scales. Outside of this kinematic region we are actually dealing with scatterings of diluted-dense system since one of the saturation scales is small. For the case of scatterings of dense-dense system of partons, the k_T factorization has not yet been proven. Nevertheless, the success of the KLN approach [2] which is based on the k_T factorization, in description of the experimental data at RHIC for gold-gold collisions suggests that the k_T factorization is currently the best tool that we have at our disposal for the processes of ion-ion scatterings.

The relation between the unintegrated gluon density ϕ_A^G and the color dipole-nucleus forward scattering amplitude has been obtained in Ref. [10]. It reads as follows:

$$\phi_A^G(x_i;\vec{k}_T) = \frac{1}{\alpha_s}\frac{C_F}{(2\pi)^3}\int d^2\vec{b}d^2\vec{r}_T e^{i\vec{k}_T\cdot\vec{r}_T}\nabla_T^2 N_A^G(x_i;r_T;b), \tag{2}$$

with notation

$$N_A^G(x_i;r_T;b) = 2N_A(x_i;r_T;b) - N_A^2(x_i;r_T;b), \tag{3}$$

where $N_A(x_i;r_T;b)$ is the dipole-nucleus forward scattering amplitude which satisfies the perturbative nonlinear small-x Balitsky-Kovchegov (BK) quantum evolution equation [11]. In the above, r_T denotes the dipole transverse size and $\vec{b}$ is the impact parameter of the scattering.

Substituting Eq. (2) into Eq. (1), and after analytically performing some integrals, we obtain [3,10],

$$\frac{d\sigma(y;p_T;\bar{B})}{dyd^2p_T} = \frac{2C_F\alpha_s(p_T)}{(2\pi)^4}\int_{B_1}^{B2} d^2\vec{B}\int d^2\vec{b}d^2\vec{r}_T e^{i\vec{p}_T\cdot\vec{r}_T} \times \frac{\nabla_T^2 N_A^G(x_1;r_T;b)\nabla_T^2 N_A^G(x_2;r_T;b_-)}{p_T^2\alpha_s(Q_A(x_1;b))\alpha_s(Q_A(x_2;b_-))}, \tag{4}$$

where $\vec{B}$ is the impact parameter between the center of two nuclei, $\vec{b}$ and $\vec{b}_- = \vec{b} - \vec{B}$ are the impact parameter between the interacting nucleons with respect to the center of two nuclei. We will see below that we can neglect the impact parameter of the produced gluon jet from the center of the nucleons.

In the above, we extended the k_T factorization given in Eq. (1) by introducing a running strong coupling α_s. For the running α_s, we employ the same prescription used in Ref. [3] for pp collisions. The saturation scale $Q_A(x_{1,2}, b)$ depends on the $x_{1,2}$ and the impact parameter and will be introduced in the following. A given centrality bin corresponds to ranges of the impact parameter $\bar{B} \in [B_1, B_2]$ of the collisions. The procedure how to select the event with a fixed $\bar{B}$ and its relation to the centrality bins is well known, see, for example, Refs. [9,12].

Notice that the relation between the unintegrated gluon density and the forward dipole-nucleus amplitude Eqs. (2) and (3) in the k_T factorization Eq. (1) is not a simple Fourier transformation which is commonly used in literature and also depends on the impact parameter. The impact-parameter dependence in these equations is not trivial and should not be in principle assumed as an overall factor. Using the general properties of high density QCD that the underlying physics depends only on the saturation scale we reconstruct the dipole-nucleus scattering amplitude in two steps. First, we choose the saturation model which effectively incorporates all known saturation properties [3] driven by the BK equation including the impact-parameter dependence of the dipole amplitude [13]. This model describes both the HERA DIS data at small x [14] and the proton-proton LHC data [3]. Second, we replace the proton saturation momentum by that of the nucleus. The dipole-nucleus scattering amplitude in our model is given by

$$N_A(x;r;b) = \begin{cases} N_0\left(\frac{\mathcal{Z}}{2}\right)^{2(\gamma_s+(1/\kappa\lambda Y)\ln(2/\mathcal{Z}))} & \text{for } \mathcal{Z}\le 2; \\ 1-\exp(-\mathcal{A}\ln^2(\mathcal{B}\mathcal{Z})) & \text{for } \mathcal{Z}>2; \end{cases} \tag{5}$$

where we defined $\mathcal{Z} = rQ_A(x;b)$, $Y = \ln(1/x)$, and $\kappa = \chi''(\gamma_s)/\chi'(\gamma_s)$ where χ is the LO Balitsky-Fadin-Kuraev-Lipatov characteristic function. The parameters $\mathcal{A}$ and $\mathcal{B}$ are determined uniquely from the matching of N_A and its logarithmic derivatives at $\mathcal{Z} = 2$. The nucleus saturation scale is given by

$$Q_A^2(x;b) = \int d^2\vec{b}' T_A(\vec{b}-\vec{b}')Q_p^2(x;b'). \tag{6}$$

In the above, the proton saturation scale Q_p is defined as

$$Q_p(x;b') = \left(\frac{x_0}{x}\right)^{\lambda/2}\exp\left\{-\frac{b'^2}{4(1-\gamma_{\rm cr})B_{\rm CGC}}\right\}, \tag{7}$$

and $T_A(B)$ denotes the nuclear thickness. We use for the nuclear thickness the Wood-Saxon parametrization [15]. Notice that for small $\mathcal{Z} \le 2$, the effective anomalous dimension $\gamma_{\rm cr} = 1 - \gamma_s$ in the exponent in the upper line of Eq. (5) rises from the BK value towards the Dokshitzer-Gribov-Lipatov-Altarelli-Parisi value. The ansatz given in Eq. (5) for a proton target was first introduced in Ref. [16]. The parameters λ, γ_s, N_0, x_0 and $B_{\rm CGC}$ are obtained from a fit to the DIS data at low Bjorken x $x < 0.01$ with a very good $\chi^2/\text{d.o.f.} = 0.92$ [14].

The saturation scale Q_A in nuclei is proportional to the density of partons in the transverse plane (see, for example, Refs. [1,2,17]) and Eq. (6) takes this fact into account. In Eq. (6), $\vec{b}'$ is the impact parameter of the color dipole with respect to the center of the proton, $\vec{b}$ is the impact parameter of the nucleon with respect to the center of the nucleus and $\vec{b} - \vec{b}'$ is, therefore, the position of the dipole with respect to the center of the nucleon. The nuclear saturation scale defined in Eq. (6) gives $Q_A^2 \approx Q_p^2 A^{1/3}$, in agreement with the basic idea of saturation and the CGC picture [1,2,17]. This is because $T_A \sim A^{1/3}$ (where A is the effective mass number of the nucleus in a given centrality) and the integral in Eq. (6) is approximately over the nucleon size. Note that since here the nucleon saturation scale depends on impact parameter, it is not then correct to define the saturation scale on a nuclear target with a simple prefactor $A^{1/3}$ scaling. In Fig. 1 we show that the impact

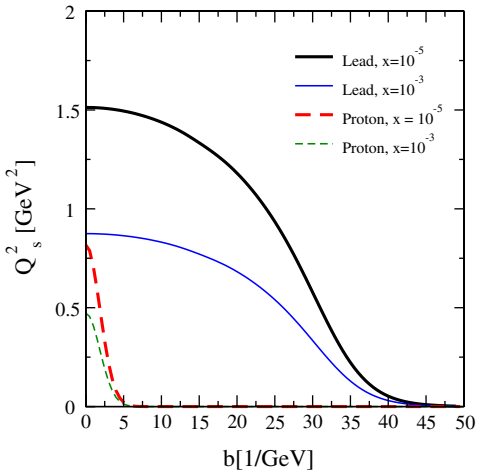

FIG. 1 (color online). The impact-parameter dependence of the saturation scale for proton and lead at $x = 10^{-3}$ and $x = 10^{-5}$.

parameter dependence of the saturation scale for proton and lead obtained from Eqs. (6) and (7) are quite different as we expected. Figure 1 demonstrates the well-known features of nucleus scattering, namely, the typical b' in Eq. (6) is much smaller than the typical $b \sim R_A$ (R_A is the nuclear radius) in the nuclear thickness.

In order to simulate the behavior of gluon density at large $x \to 1$, we product the unintegrated gluon density with $(1-x)^4$ as prescribed by quark counting rules and the HERA data on DIS at large x [3]. Notice that the contribution of $(1-x)^4$ correction at $\sqrt{s} = 5.5$ TeV for AA collisions and $\eta \leq 4.5$ is less than 4%, and for $4.5 < \eta < 6$ is less than 13%. Therefore, the main contribution of the unintegrated gluon density at the LHC high energy in the kinematic region considered here for both AA and also pp collisions [3] comes from the small x region where the saturation physics is important. For the importance of the saturation effects in pA collisions at the LHC, see Ref. [18].

The k_T factorization Eqs. (1) and (4) gives the cross section of radiated gluon minijets with zero mass while what is actually measured experimentally is the distribution of final hadrons. We therefore should model the nonperturbative hadronization stage of gluon minijets. We employ the local parton-hadron duality principle [19], namely, the hadronization is a soft process and cannot change the direction of the emitted radiation. Hence, the form of the rapidity distribution of the minijet and the produced hadron are different only with a numerical factor $\mathcal{C}$. It is well known that the general assumption about hadronization leads to the appearance of mass of the minijet which is approximately on average equal to $m_{\rm jet}^2 \simeq 2\mu\langle p_T\rangle$ [2,3] where μ is the scale of soft interaction. The minijet mass $m_{\rm jet}$ effectively incorporates the nonperturbative soft prehadronization in the pseudorapidity space and can be approximately related to the saturation scale [3]. Accordingly, one should also correct the kinematics every where in Eq. (4) due to the presence of a nonzero minijet mass, namely, replacing $p_T \to \sqrt{p_T^2 + m_{\rm jet}^2}$ in x_1, x_2 and also in the denominator of $1/p_T^2$. Finally, in order to take account of the difference between rapidity y and the measured pseudorapidity η, we employ the Jacobian transformation between y and η [3].

Following Ref. [3], in the spirit of the geometrical-scaling property of the scattering amplitude, we obtain the charged-particle multiplicity distribution at a fixed centrality but various energies from the corresponding minijet cross section Eq. (4) divided by the average area of interaction $\sigma_s = \mathcal{M}\pi\langle\vec{b}_{\rm jet}^2\rangle = \mathcal{M}\pi\langle b^2 + b_-^2\rangle$. In a similar way, in order to obtain the charged-particle multiplicity distribution at various centrality bins but a fixed energy, we divide the minijet cross section integrated in ranges of $\bar{B} \in [B_1, B_2]$ with the corresponding relative interaction area $\sigma_s = \mathcal{M}\pi(B_2^2 - B_1^2)$.

III. DISCUSSION AND PREDICTIONS

We have only two unknown parameters in our model: the overall factor $\frac{K\mathcal{C}}{\mathcal{M}}$ and the soft scale μ introduced in the definition of minijet mass. We also introduced a K factor which incorporates the discrepancy between the exact calculation with our formulation. These two phenomenological parameters are fixed at RHIC energy $\sqrt{s} =$ 200 GeV for Au-Au 0–6% centrality. Then our results at other energies and various centralities can be considered as free-parameter predictions. The sensitivity of our results to various μ is shown in Fig. 2 (top) at $\sqrt{s} = 200$ GeV. The preferred value of μ in Pb-Pb collisions is approximately of order the current-quark mass and is smaller than the corresponding value of $\mu \approx m_\pi$ in pp collisions [3]. The decrease in the value of the soft scale in a denser medium is in accordance with the notion of asymptotic deconfinement that the confinement radius increases with density. The preferred value of the soft scale in AA collisions is very close to what was obtained in Ref. [20] for the value of $\Lambda_{\rm QCD}$ at moderate densities. Loosely-speaking, the smallness of μ for AA collisions compared to the pp collisions is due to the fact that the minijet mass reduces in a denser medium despite the fact that the saturation scale increases. We checked that for Pb-Pb and pp collisions a fixed minijet mass about 0.14–0.2 and 0.4–0.5 GeV, respectively, gives similar results to the case that the minijet mass runs with the saturation scale. As we already pointed out the minijet mass mimics the properties of the soft nonperturbative prehadronization stage and a different value for μ in AA collisions is simply due to the fact that the soft prehadronization stage in AA collisions is different from the corresponding one in pp collisions.

The main sources of theoretical uncertainties in our approach stem from assuming a fixed μ (or a fixed $m_{\rm jet}$) and the prefactor $\frac{K\mathcal{C}}{\mathcal{M}}$ for all energies, rapidities and centralities. The experimental errors in the data points taken for

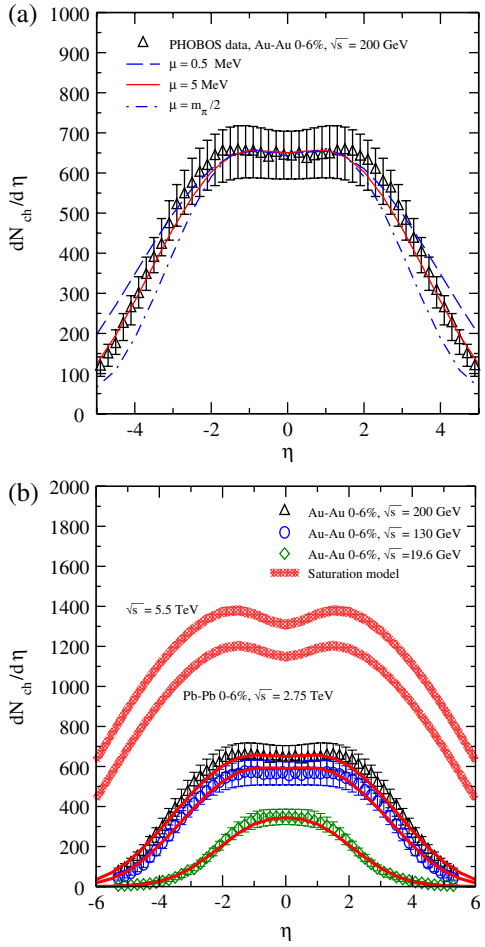

FIG. 2 (color online). Top: The effect of the soft scale μ is shown at $\sqrt{s} = 200$ GeV. Lower: Pseudorapidity distribution of charged particles produced in Au-Au and Pb-Pb central 0–6% collisions at RHIC $\sqrt{s} = 19.6$, 130, 200 GeV and the LHC energies $\sqrt{s} = 2.75$, 5.5 TeV. The band indicates less than 3% theoretical error coming from uncertainties related to normalization and modeling the minijet mass. The experimental data are from the PHOBOS Collaboration [24].

fixing these two unknown parameters also induce some uncertainties. Moreover, we employed a Glauber based approach to relate the centrality bins, number of participant and the cut in the impact parameters [9,12]. This formulation agreed with the RHIC data on number of participant within error bars, but we expect some uncertainties in the Glauber formulation mainly due to its over-simplicity. In the Glauber formalism one should also assume the value of inelastic nucleon-nucleon cross section $\sigma_{\rm nn}^{\rm inel}$ (without diffractive components) from outset. Here we used the values obtained in Ref. [21]: $\sigma_{\rm nn}^{\rm inel} = 64.8$, 58.5, 42, 41, 30 mb for $\sqrt{s} = 5500$, 2750, 200, 130, 19.6 GeV, respectively. Notice that the nuclear saturation scale defined in Eq. (6) can be in principle different with exact one with extra factor. In order to estimate this uncertainty, we checked that a factor of 2 difference in the definition of Eq. (6) (namely $Q_A \to 2Q_A$) will change our result less than 5% at the LHC. Overall, including all the above-mentioned possible theoretical uncertainties, we expect less than 7% theoretical error in our calculations at the LHC energies. The theoretical bar in Fig. 3 and 4 only show about 3% theoretical error.

In Fig. 2 (lower), we show our predictions at lower RHIC energies $\sqrt{s} = 19.6$ and 130 GeV in Au-Au collisions, and also for the LHC energies $\sqrt{s} = 2.75$ and 5.5 TeV in Pb-Pb collisions for 0–6% centrality bin.

In Fig. 3, we show the charged-particle multiplicity at various centrality bins for RHIC and the LHC high energy. As we already stressed we only used RHIC data at $\sqrt{s} = 200$ GeV for 0–6% centrality bin in order to fix two unknown parameter of our model. Therefore, the description of other RHIC data here can be considered as predictions. Overall, our approach gives a very good description of RHIC multiplicity data as a function of rapidity, centrality, number of participant and energy, see Figs. 2–5.

In Fig. 4 we show the energy dependence of $dN_{pp}/d\eta$, $dN_{AA}/d\eta$ and $(2/N_{\rm par})dN_{AA}/d\eta$ at midrapidity $\eta = 0$ for

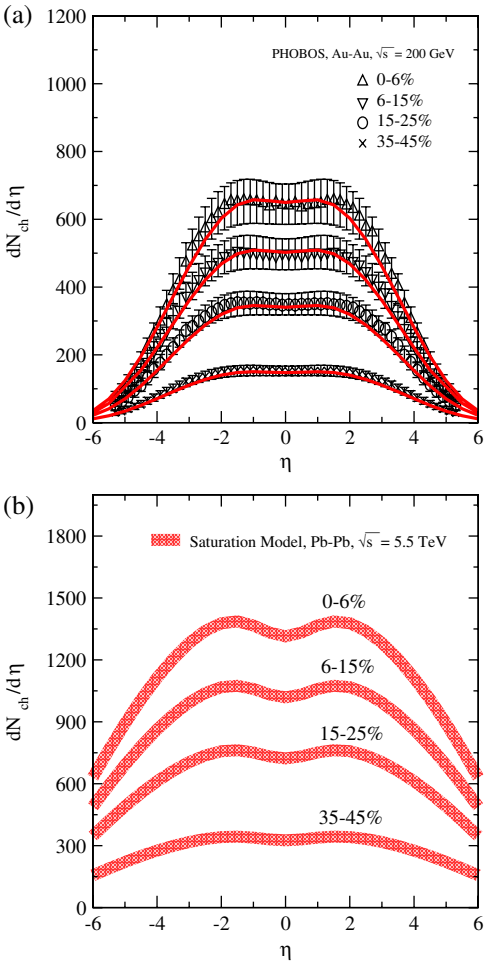

FIG. 3 (color online). The pseudorapidity dependence at RHIC $\sqrt{s} = 200$ GeV (top) and the LHC $\sqrt{s} = 5.5$ TeV (lower) at different centrality bins. The band indicates less than 3% theoretical errors. The experimental data are from the PHOBOS Collaboration [24].

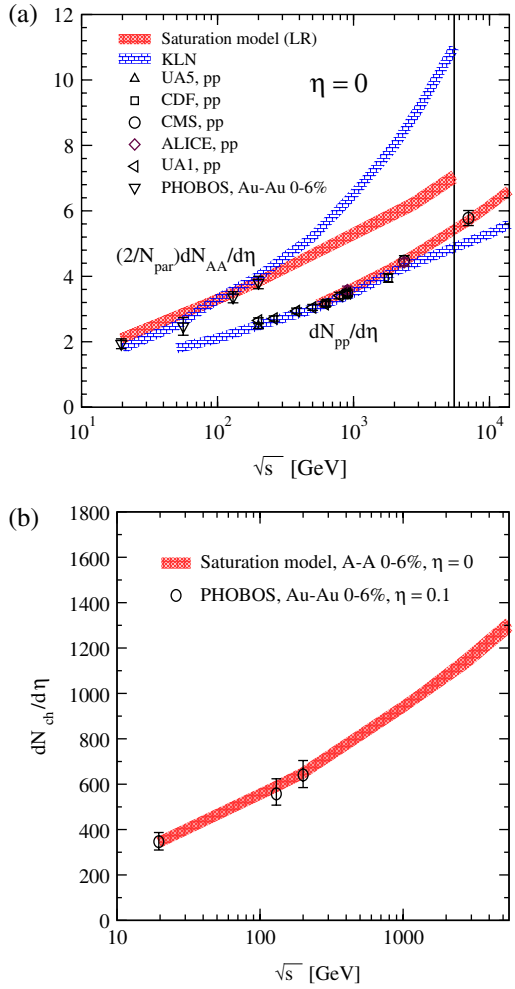

FIG. 4 (color online). Energy dependence of the charged hadrons multiplicity at midrapidity $\eta = 0$ in central collisions in pp and AA collisions. The theoretical curve saturation model (LR) is our prediction. The band indicates less than 3% theoretical errors. The total theoretical uncertainties is less than 7%, see the text for the details. We also show the KLN prediction [9] with the same error band as ours. The experimental data are from [4–6,24,25].

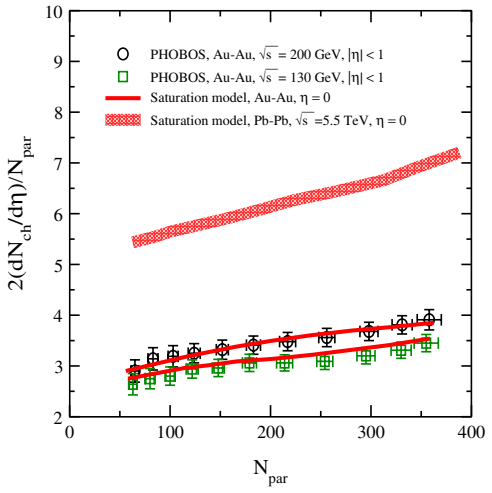

FIG. 5 (color online). The scaled pseudorapidity density as a function of number of participant $N_{\rm par}$ at midrapidity for Au-Au at $\sqrt{s} = 130$, 200 GeV and for Pb-Pb at $\sqrt{s} = 5.5$ TeV. The experimental data are from the PHOBOS Collaboration [26].

central collisions (where $N_{\rm par}$ denotes the number of participant for a given centrality). In Fig. 4, we also show our predictions for the charged-hadron multiplicity in pp collisions. We should emphasize again that the main difference in our formulation for the case of pp and AA collisions is only due to the employed different saturation scale for a proton and a nuclear target Eqs. (7) and (6) [see Fig. 1] and the rest of the formulation is the same. This is in accordance with the notion of universality of the saturation physics which can be further tested at the LHC. In Fig. 4, we show that the recent data from CMS at $\sqrt{s} = 7$ TeV remarkably confirms our predictions for pp collisions. Our predictions for $dN_{AA}/d\eta$ at midrapidity $\eta = 0$ for central Pb-Pb collisions (for $B \leq 3.7$ fm or approximately 0–6% centrality bin) for $\sqrt{s} = 2.75$ and 5.5 TeV are 1152 ± 81 and 1314 ± 92, respectively. Similar results was also suggested in Ref. [22] based on the numerical solution of the BK equation with running strong-coupling with the model assumption that the dipole amplitude does not depend on the impact parameter. However, in this paper [22], the relation between the unintegrated gluon density and the forward dipole-nucleus amplitude in the k_T factorization was taken a simple Fourier transformation instead of Eqs. (2) and (3). The predictions of other approaches at the LHC can be found in Ref. [23].

In Fig. 5, we show $(2/N_{\rm par})dN_{AA}/d\eta$ as a function of number of participant for RHIC and the LHC energies at midrapidity.

Notice that the KLN approach similar to here is also based on the k_T factorization. Both approaches describe the RHIC data but provide rather different predictions at the LHC. In Fig. 4, we also show the KLN predictions for both pp and AA collisions. Obviously, the KLN predictions underestimated the pp multiplicity data at the LHC $\sqrt{s} = 7$ TeV (in contrast to our predictions) while it overestimates the multiplicity for AA collisions compared to our predictions. The main differences between our approach and the KLN one is that we used explicitly the impact-parameter dependent form of the k_T factorization and employed the correct relation between the unintegrated gluon density and the forward dipole-nucleon amplitude Eqs. (2) and (3). Then we employed an impact-parameter dependent saturation model which gives a good description of HERA data at small x. In this sense, we did not have any freedom to model the saturation dipole-proton amplitude at RHIC or the LHC. The key difference between our approach and the KLN one is the fact that we rely on Eq. (6) to determine the saturation scale for nucleus while in the KLN approach [9] the energy dependence was used to

obtain the saturation scale for nucleus at the LHC from the one at RHIC.

IV. CONCLUSIONS

We developed a saturation approach, based on the CGC theory, which describes DIS data at HERA [14], hadron production at the LHC [13] in pp collisions and at RHIC in AA collisions (this paper). In this approach we treat in the same way proton and nuclear target considering that the only difference between them is the value of the saturation scale. The nonperturbative stage of the jet-hadronization was described in the same scheme for both proton and nuclear target, minimizing the uncertainties in prediction that could stem from this stage. We provided here various quantitative predictions including the rapidity, centrality and energy dependencies of the inclusive charged-hadron multiplicity in AA collisions at the LHC. We believe that our predictions for nucleus-nucleus collisions at the LHC will be a crucial test of the CGC approach.

ACKNOWLEDGMENTS

We are thankful to J F. Grosse-Oetringhaus, Y. Kovchegov, and B. Zajc for useful communication. This work was supported in part by the Conicyt Programa Bicentenario under Contract No. PSD-91-2006 and the Fondecyt (Chile) under Grant Nos. 1090312 and 1100648.

[1] L. V. Gribov, E. M. Levin, and M. G. Ryskin, Phys. Rep. **100**, 1 (1983); A. H. Mueller and J. Qiu, Nucl. Phys. **B268**, 427 (1986); L. McLerran and R. Venugopalan, Phys. Rev. D **49**, 2233 (1994); **49**, 3352 (1994); **50**, 2225 (1994); **53**, 458 (1996); **59**, 094002 (1999); I. Balitsky, Nucl. Phys. **B463**, 63 (1996) A. H. Mueller, Nucl. Phys. **B415**, 373 (1994); **B437**, 107 (1995); Y. V. Kovchegov, Phys. Rev. D **60**, 034008 (1999); J. Jalilian-Marian, A. Kovner, A. Leonidov, and H. Weigert, Phys. Rev. D **59**, 014014 (1998); Nucl. Phys. **B504**, 415 (1997); J. Jalilian-Marian, A. Kovner, and H. Weigert, Phys. Rev. D **59**, 014015 (1998); A. Kovner, J. G. Milhano, and H. Weigert, Phys. Rev. D **62**, 114005 (2000); E. Iancu, A. Leonidov, and L. D. McLerran, Phys. Lett. B **510**, 133 (2001); Nucl. Phys. **A692**, 583 (2001); E. Ferreiro, E. Iancu, A. Leonidov, and L. McLerran, Nucl. Phys. **A703**, 489 (2002); H. Weigert, Nucl. Phys. **A703**, 823 (2002).

[2] D. Kharzeev, E. Levin, and M. Nardi, Nucl. Phys. **A730**, 448 (2004); **A743**, 329(E) (2004).Phys. Rev. C **71**, 054903 (2005); D. Kharzeev and E. Levin, Phys. Lett. B **523**, 79 (2001); D. Kharzeev and M. Nardi, Phys. Lett. B **507**, 121 (2001).

[3] E. Levin and A. H. Rezaeian, Phys. Rev. D **82**, 014022 (2010).

[4] CMS Collaboration, Phys. Rev. Lett. **105**, 022002 (2010).

[5] V. Khachatryan *et al.* CMS Collaboration, J. High Energy Phys. 02 (2010) 41.

[6] (ALICE Collaboration), Eur. Phys. J. C **65**, 111 (2010); ALICE Collaboration, Eur. Phys. J. C **68**, 89 (2010).

[7] ATLAS Collaboration, Phys. Lett. B **688**, 21 (2010).

[8] L. McLerran and M. Praszalowicz, arXiv:1006.4293.

[9] D. Kharzeev, E. Levin, and M. Nardi, Nucl. Phys. **A747**, 609 (2005).

[10] Y. V. Kovchegov and K. Tuchin, Phys. Rev. D **65**, 074026 (2002).

[11] I. Balitsky, Phys. Rev. D **60**, 014020 (1999); Y. V. Kovchegov, Phys. Rev. D **60**, 034008 (1999).

[12] D. Kharzeev, C. Lourenco, M. Nardi, and H. Satz, Z. Phys. C **74**, 307 (1997); U. A. Wiedemann, in *Proceedings of the European School of High-Energy Physics 2007, Trest, Czech Republic, 19 Aug - 1 Sep 2007*, edited by N. Ellis and R. Fleischer, (CERN, Geneva, 2008).

[13] E. Levin and K. Tuchin, Nucl. Phys. **B573**, 833 (2000).

[14] G. Watt and H. Kowalski, Phys. Rev. D **78**, 014016 (2008).

[15] C. W. De Jagier, H. De Vries, and C. De Vries, At. Data Nucl. Data Tables **14**, Nos. 5-6479 (1974).

[16] E. Iancu, K. Itakura, and S. Munier, Phys. Lett. B **590**, 199 (2004).

[17] A. H. Mueller, Nucl. Phys. **A724**, 223 (2003); Nucl. Phys. **B558**, 285 (1999); D. Kharzeev, E. Levin, and L. McLerran, Phys. Lett. B **561**, 93 (2003); E. M. Levin and M. G. Ryskin, Nucl. Phys. **B304**, 805 (1988); Sov. J. Nucl. Phys. **41**, 472 (1985).

[18] D. Kharzeev, Y. V. Kovchegov, and K. Tuchin, Phys. Lett. B **599**, 23 (2004); A. H. Rezaeian and A. Schäfer, Phys. Rev. D **81**, 114032 (2010).

[19] Y. L. Dokshitzer, V. A. Khoze, and S. I. Troian, J. Phys. G **17**, 1585 (1991).

[20] D. H. Rischke, D. T. Son, and M. A. Stephanov, Phys. Rev. Lett. **87**, 062001 (2001).

[21] E. Gotsman, E. Levin, U. Maor, and J. S. Miller, Eur. Phys. J. C **57**, 689 (2008).

[22] J. L. Albacete, Phys. Rev. Lett. **99**, 262301 (2007).

[23] N. Armesto *et al.*, J. Phys. G **35**, 054001 (2008); N. Armesto, arXiv:0903.1330.

[24] PHOBOS Collaboration, Phys. Rev. Lett. **91**, 052303 (2003).

[25] S. Eidelman (Particle Data Group Collaboration), Phys. Lett. B **592**, 1 (2004); UA1 Collaboration, Nucl. Phys. **B335**, 261 (1990); UA5 Collaboration, Z. Phys. C **33**, 1 (1986); CDF Collaboration, Phys. Rev. D **41**, 2330 (1990); CDF Collaboration, Phys. Rev. Lett. **61**, 1819 (1988); A. M. Rossi *et al.*, Nucl. Phys. **B84**, 269 (1975).

[26] PHOBOS Collaboration, Phys. Rev. C **65**, 061901(R) (2002).